ARTICLE

Testing the reversible insertion of magnesium in cationic-deficient manganese oxy-spinel through a concentration cell

Received 00th January 20xx,
Accepted 00th January 20xx

DOI: 10.1039/x0xx00000x

Alejandro Medina,[a] Ana I. Rodríguez,[a] Carlos Pérez-Vicente[a] and Ricardo Alcántara[a]*

Magnesium-ion batteries could be competitive against lithium-ion batteries, but it is needed to verify the reversible intercalation of magnesium in the framework of the host material. A concentration cell has been built by using electrodes with different concentrations of magnesium ion in the cubic spinel $Mg_xMn_2O_4$. For this purpose, firstly cations were partially extracted from $MgMn_2O_4$ by acid-treatment. This concentration cell is used to test the reversible intercalation of magnesium and the effect of the cationic vacancies. The theoretical results on the percolation energy can explain the lower polarization experimentally observed in the voltage curve of the acid-treated sample.The reversible capacity (ca. 115 mAh g^{-1}) is preserved after charge-discharge cycling.

Introduction

Lithium batteries have been successfully commercialized from the 1990's decade. However, these batteries are not exempt from drawbacks, such as the high cost and limited mineral resources. Sodium and magnesium batteries are probably the most promising to replace lithium batteries.[1-4]

One of the major hurdles for magnesium batteries is the lack of materials that undergo reversible (de)intercalation of magnesium. The experimental and theoretical studies of the mechanism of (des)insertion of Mg can help to design stable structures allowing reversible charge/discharge.[5]

The manganese oxides with spinel-type structure (AB_2O_4) are among the most interesting materials for rechargeable magnesium batteries.[6-13] However, the intercalation of divalent ions, such as zinc and magnesium, into the spinel can be a subject to debate. In addition, very small particles with high surface area and defects can promote Mg-ion migration and better rate capability.[11]

Oxidation treatments and acid treatments can be used to remove Mg ions from some compounds, forming new compounds and investigating the (de)magnesiation processes. For example, $Mg_xMn_2O_4$ and several phases of MnO_2 can be obtained starting from $MgMn_2O_4$.[14] Although the chemical treatments can be interesting and useful, one cannot extrapolate directly these results to the electrochemical behaviour. It is needed to employ also theoretical calculations and electrochemical experiments. Unfortunately, the experimental study of the electrochemical behaviour in Mg cells is not exempt from difficulties.

One of the main problems to explore the intercalation of magnesium is the suitability of the reference electrode and/or counter electrode, and the compatibility of all the electrodes with the electrolyte solution.[15] The structural stability of the Mg counter electrode and its compatibility with the electrolyte influences on the electrochemical cycling.[16] The reversibility of Mg anode in moisture contaminated nonaqueous electrolyte is infeasible, although the water molecules can help to stabilize the structure of layered-type manganese oxide.[5,11,17] $Mg(ClO_4)_2$ is not very compatible with the reversible plating of Mg in the counter electrode. The anion $TFSI^-$ of the salt magnesium bis(trifluoromethylsulfonyl)amide is oxidatively decomposed near 3 V. The activated carbon electrode can adsorb anions and modify the electrolyte solution. The desolvation of magnesium is particularly difficult with dimethoxyethane solvent.[18] All these effects and parasitic reactions can interfere in the study of the main intercalation reaction. Thus, new electrochemical procedures are needed to suppress side-reactions and interferences, and to explore properly the intercalation of magnesium. For example, Pt mesh has been used to replace Mg as a counter electrode.[5,14]

It is known that the structure collapse of the manganese oxides provoked by the local change of the MnO_6 octahedra during the oxidation/reduction can be responsible of the capacity loss.[5,15]

It is important to determine theoretically and experimentally the factors that can help to achieve structure stability, easy and rapid (des)intercalation of magnesium and efficient charge/discharge cycling. Having all this in mind, both theoretical calculations and experimental studies are carried out here to study the (de)intercalation of Mg into the spinel structure and the effect of the vacancies. We have prepared nanosized $MgMn_2O_4$ at relatively low temperature (400°C), and then we have treated with acid this oxy-spinel to remove

[a] Departamento de Química Inorgánica e Ingeniería Química, Instituto Universitario de Investigación en Química Fina y Nanoquímica (IUNAN), Universidad de Córdoba, Campus de Rabanales, Edificio Marie Curie, E-14071 Córdoba, Spain.
[b] * Corresponding: ralcantara@uco.es

† Footnotes relating to the title and/or authors should appear here.
Electronic Supplementary Information (ESI) available: [Details of calculations. TEM. Micrographs. Impedance spectroscopy results]. See DOI: 10.1039/x0xx00000x

cations. Through this new experimental procedure, two electrode materials $Mg_xMn_2O_4$ with different concentrations of Mg are available to study the intercalation of magnesium in the spinel structure, avoiding the use of a different compound as counter electrode and with no interference of other electrode materials. As a fundamental novelty, we unveil the role played by the cationic vacancies.

Materials and methods

Synthesis

$MgMn_2O_4$ was prepared by following a modification of Pechini's method.[6] Magnesium nitrate, manganese nitrate, citric acid and ethyleneglycol were dissolved in water. After heating to evaporate the water, the resulting slurry was calcinated at 200°C, then grinded and finally annealed at 400°C for 10 h in air atmosphere.

The acid-treatment of $MgMn_2O_4$ was carried out with nitric acid solution at pH = 2 for two hours.[6,7] The resulting sample was rinsed with distilled water and dried at 90°C under vacuum.

Microstructure and composition

The structures of the samples were characterized by XRD using a Bruker D8 Discover A25 instrument with CuKα radiation and Ge monochromator. The lattice cell parameters and the crystallite size were calculated using the Topas software and the full pattern matching method.

The microstructure of the particles was studied by Transmission Electron Microscopy (TEM) using a JEM-1400 instrument.

The chemical compositions (Mg and Mn elements) of the electrode active materials were analysed by X-ray fluorescence (XRF) employing a Rigaku Primus IV instrument.

Electron Spin Resonance (ESR) spectra were recorded at room temperature in a Bruker EMX instrument, operating at X-band and 9.75 GHz.

Electrochemistry

To carry out electrochemical experiments, a VMP instrument and three-electrode cells were employed. The Swagelok-type cells with T-shape were assembled in an Ar-filled glovebox. The electrodes were formed by active material (80%), binder (PVDF, 10%) and carbon black (10%) pressed on a Ti (Goodfellow) current collector. A piece of Mg (Panreac) was used as a reference electrode. The electrolyte solution was 1 M anhydrous $MgClO_4$ (Sigma-Aldrich) in dry acetonitrile (ACN) (Sigma-Aldrich) impregnated in Whatman glass fibre papers. The solvent was dried with molecular sieve.

For the sake of comparison, the electrochemistry was also studied using Mg as counter electrode and another piece of Mg as reference electrode, and 0.5 M $Mg(TFSI)_2$ in dimethoxyethane (DME) as electrolyte solution.

For the galvanostatic experiments, the imposed lower cut-off voltage of the working electrode was 0.5 V vs. Mg reference electrode. For the charge (oxidation) process, a double limit was imposed: voltage and charge capacity. With this double limit, the risk of parasitic reactions interfering with the main reaction is decreased, although the apparent capacity is limited.

Calculations

The structure calculations were performed within the density functional theory (DFT), as implemented in the CASTEP code.[19] We use the Generalized-Gradient Approximation (GGA) with the PBEsol correlation potential, and "on-the-fly" generated pseudopotentials of CASTEP code. The internal coordinates were optimized using the BFGS algorithm, while the energy minimization was carried out using a density-mixing scheme with a conjugate-gradient Pulay solver. The cut-off energy was fix at 550 eV. Spin polarized calculations were performed in all cases. The selected k-point mesh was of ca. 0.07 $Å^{-1}$, according to the Monkhorts-Pack scheme. The convergence conditions were: energy, 10^{-5} eV $(atom)^{-1}$; max. force, 0.03 eV $Å^{-1}$; max. stress, 0.05 GPa and max. displacement, 10^{-3} Å. The GGA+U correction was introduced by using the simplified, rotationally invariant approach as implemented in Castep. We used the value U_{eff} = 3.9 eV for the d-state of Mn atoms.[3]

Bond Valence Energy Landscape approach was used to estimate the percolation energy, as implemented in the software Bond STR included in the FullProf Suite Package. In the calculation, we used soft bond valence parameters (softBV).

Results and discussion

Theoretical calculations

Through theoretical calculations within the density functional theory, the structure optimization of $MgMn_2O_4$ confirms the tetragonal distortion of the normal spinel, according to the Jahn-Teller distortion induced by Mn^{3+}. The unit cell parameters are a = 5.745 Å and c = 9.426 Å, in agreement with previously published results,[5-8] and with our experimental values (see below). The full demagnesiation involves a tetragonal to cubic transition (a = 8.158 Å), as the Jahn-Teller distortion is no longer present. It is accompanied by a decrease of the cell volume of 12.7 %, in agreement with previous calculations.[3] We also explored the partially demagnesiated phases $Mg_{0.75}Mn_2O_4$, $Mg_{0.5}Mn_2O_4$ and $Mg_{0.25}Mn_2O_4$ but no special stability was found, as evidenced in the Hull diagram shown in Fig. 1a. These phases were obtained by progressively eliminating Mg atoms from the $Mg_4Mn_8O_{16}$ tetragonal unit cell. The theoretical results (Fig. 1a) about the instability and disproportionation of the intermediate compositions $Mg_xMn_2O_4$ ($0 < x < 1$) agrees well with the results previously reported by other authors.[20] However, this thermodynamic process may be slow, and the intermediate compositions could be formed.

On the other hand, the insertion of more magnesium, with $1 < x < 2$ in $Mg_xMn_2O_4$, would yield to the formation of the ordered rock-salt structure, accompanied by an expansion of 6 % of the cell volume, as compared with $MgMn_2O_4$.

The theoretical calculated voltage-composition curve for $Mg_xMn_2O_4$ is shown in Fig. 1b. The voltage for the extraction of Mg from $MgMn_2O_4$ to yield MnO_2 is ca. 2.8 V vs. Mg^{2+}/Mg, in agreement with previous calculations.[3] The insertion of Mg to give $Mg_2Mn_2O_4$ is expected at ca 2.0 V.

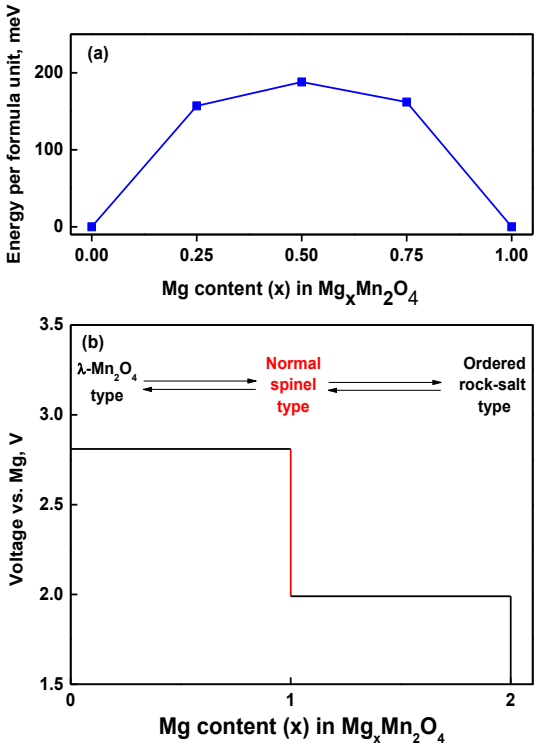

Fig. 1 Results of theoretically calculations. (a) Hull diagram. (b) Voltage as a function of Mg content in $Mg_xMn_2O_4$.

Acid-treatment and microstructure

According to the TEM micrographs (Fig. S2), the prepared samples are powders composed by nanometric particles with irregular morphology. The diameter of the particles is around 10-50 nm.

The structure results obtained from the XRD patterns agree well with the theoretical calculations. The XRD pattern of $MgMn_2O_4$ (Fig. 2a) can be indexed in the space group $I4_1/amd$ (141) of a tetragonal spinel, and the obtained lattice cell parameters (a = 5.7170(28) Å and c = 9.2297(56) Å) agree well with the literature[5-7] and with our theoretical calculations. The broad reflections indicate a small crystallite size, and the calculated average value is L = 25 nm. The relatively high intensity of the reflection (011) compared to (211) is indicative of an ordered phase $(Mg^{2+})_T[Mn^{3+},Mn^{3+}]_OO_4$, with no or small migration of Mg from tetrahedral to octahedral site.[7,21]

According to the XRF analysis, the experimental ratio Mg/Mn changes from 0.5 to 0.15, before and after acid-treatment, respectively. For the acid-treated sample, the Bragg reflections becomes even more broadened and the XRD pattern can be indexed in a cubic space group $Fd\bar{3}m$ (Fig. 2b). The broaden reflections also suggest a more defective structure. The resulting cell parameter is a = 8.12(08) Å, and the crystallite size is L = 18 nm. Thus, the XRD pattern is like the pattern of λ-MnO_2 phase, irrespectively of the remaining magnesium. The lack of XRD reflections of the tetragonal spinel (Fig. 3b), would agree well with a single phase. However, after looking at the broad reflections we cannot completely discard the presence of a small amount of the tetragonal phase. In any case, our goal here is to create cationic vacancies in the spinel structure, not to obtain pure λ-MnO_2.

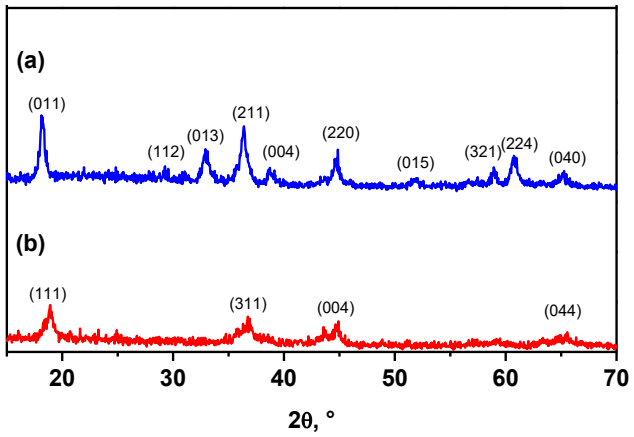

Fig. 2 XRD patterns before (a) and after acid treatment (b). The Miller indexes of the Bragg reflections are indicated

The ESR spectroscopy is very sensitive to the changes of the oxidation states of paramagnetic ions and to the interactions between them. The ESR spectrum of $MgMn_2O_4$ (Fig. 3a) agrees well with the literature and can be interpreted on the basis of the analysis of Azzoni et al.[22] The very broad signal (ΔH ≈ 2700 G) and g = 2.06 observed for $MgMn_2O_4$ is assigned to all the Mn^{3+} (^5D) ions in octahedral coordination with a strong tetragonal distortion and in an environment rich of paramagnetic ions. The particle size dispersion can contribute to the broadness of the line. There is small narrower signal centred at g = 1.96 with smaller intensity which can be due to a very small degree of inversion, where the diamagnetic Mg^{2+} ions in octahedral sites break the magnetic interactions between the Mn^{3+}. An alternative explanation could be that a little population of very small particles contribute to this small signal, as it was observed for manganese ferrites.[23] After acid treatment (Fig. 3b), the ESR line is modified and becomes more complex, suggesting heterogeneity in the manganese ions, and it agrees very well with the disproportionation reaction. There is a signal with broadening ΔH ≈ 700 G and another signal even broader (ΔH ≈ 2500 G). The ions Mn^{4+} (^4F), Mn^{3+} and Mn^{2+} (^6S) can contribute to these signals. More probably the narrower signal is due to Mn^{4+} ions near to others Mn^{4+}, because the superexchange interactions Mn^{4+}-Mn^{4+} narrow the signal.[24] The observed change of the ESR spectra with the Mg/Mn ratio is somewhat equivalent to the results previously reported when the Li/Mn ratio in $Li_{1+x}Mn_{2-x}O_4$ is changed and cationic vacancies are created.[25, 26]

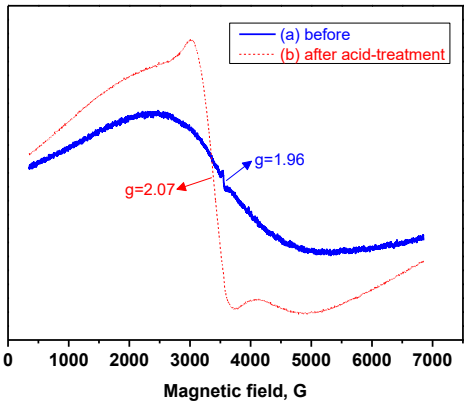

Fig. 3 ESR spectra before (a) and after acid treatment (b).

The acid-treatment of $MgMn_2O_4$ and the consequent partial demagnesiation is happening by disproportionation of Mn(III) through the Hunter's mechanism.[6,7] The disproportionation reaction of Mn(III) into Mn(IV) and Mn(II) involves deviation from the stoichiometric composition and dissolution of Mn(II) ions:

$(1+x)MgMn_2O_4(s) + (8x)H^+(aq.) \rightarrow Mg_{1-x}Mn_2O_4(s) + (2x)Mn^{2+}(aq.) + (2x)Mg^{2+}(aq.) + (4x)H_2O(l)$ (1)

MnO and MgO are soluble in the acidic solution, while Mn^{4+} is left behind in the spinel,[7] and the formula of the product has been normalized as $Mg_{1-x}Mn_2O_4$. It is usual to find that some Mg ions remain in the lattice of the manganese oxide, and the resulting x-value depends on parameters such as the time of the acid-treatment and the disorder in the pristine spinel.[7,14] The elimination of Mn(III) ions by disproportionation suppresses the cooperative tetragonal distortion of the unit cell which is induced by the local Jahn-Teller effect of Mn(III). The remaining Mg ions suggest that their diffusion in the spinel is a slower process compared with lithium in $LiMn_2O_4$. $Mg_{1-x}Mn_2O_4$ is expected to be a tetragonal spinel for Mn oxidation state below +3.5, and a cubic spinel beyond +3.5, but a cubic spinel also can be observed slightly below +3.5 due to the cationic disorder.[7] The small particle size of the pristine sample also could contribute to have a single phase and a homogeneous sample.

The acid treatment is not just a demagnesiation process. The creation of cationic vacancies (both magnesium and manganese) can decrease the cation-cation repulsions, increase the magnesium mobility, decrease the voltage polarization and improve the electrochemical behaviour, as it is discussed below.

Mg cell

The electrochemistry of the spinel $MgMn_2O_4$ before and after acid-treatment in Mg cell is summarized in Fig. 4. The galvanostatic cycling was started by a discharge process (reduction at the working electrode), as it is usual. It is observed that the capacity of $MgMn_2O_4$ (Fig. 4a) is lower (25 mAh g^{-1}) in the first discharge compared to $Mg_{0.3}Mn_2O_4$ (130 mAh g^{-1}) (Fig. 4b). This result illustrates the little ability of the composition $MgMn_2O_4$ to intercalate more Mg. In the successive cycles, the capacity of the acid-treated-sample is also higher. In addition, the charge voltage of raw $MgMn_2O_4$ (Fig. 4a) is lower compared to $Mg_{0.3}Mn_2O_4$ (Fig. 4b).

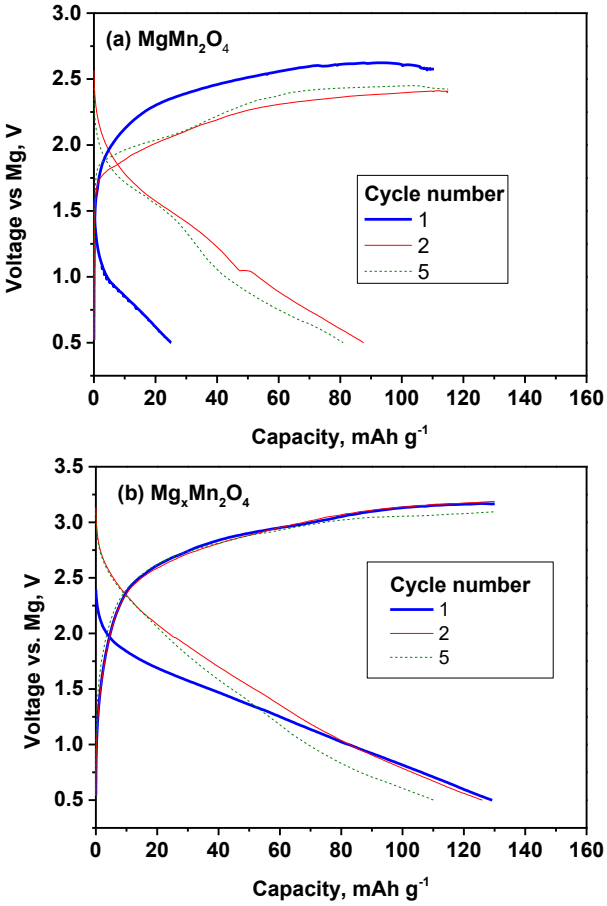

Fig. 4 Voltage curves for $MgMn_2O_4$ in Mg cell before (a) and after acid-treatment (b). Electrolyte: $Mg(TFSI)_2$ in DME. Current density: 5 mA g^{-1}.

These results strongly suggest that the direct reduction of $MgMn_2O_4$ can be deleterious for its electrochemical behaviour, and that the formation of the phase Mg_2MnO_4 phase should be avoided, in good agreement with the theoretical calculations. Otherwise, the irreversible decomposition of $TFSI^-$ could contribute to the apparent capacity near ca. 3 V and to affect to the measured voltage. The discrepancies between the theoretically calculated voltage and the experimental voltage can be influenced by parasitic reactions (electrolyte decomposition) and formation of a blocking layer in the reference electrode. In fact, Mg is rather a pseudoreference electrode. In addition, the stability of the Mg counter electrode also can influence on the cycling behaviour of the whole cell.[16] Consequently, a different electrochemical cell is employed here below to study more properly this spinel, and particularly the effect of the cationic vacancies within the range of composition corresponding to the cubic structure.

Cell of concentration

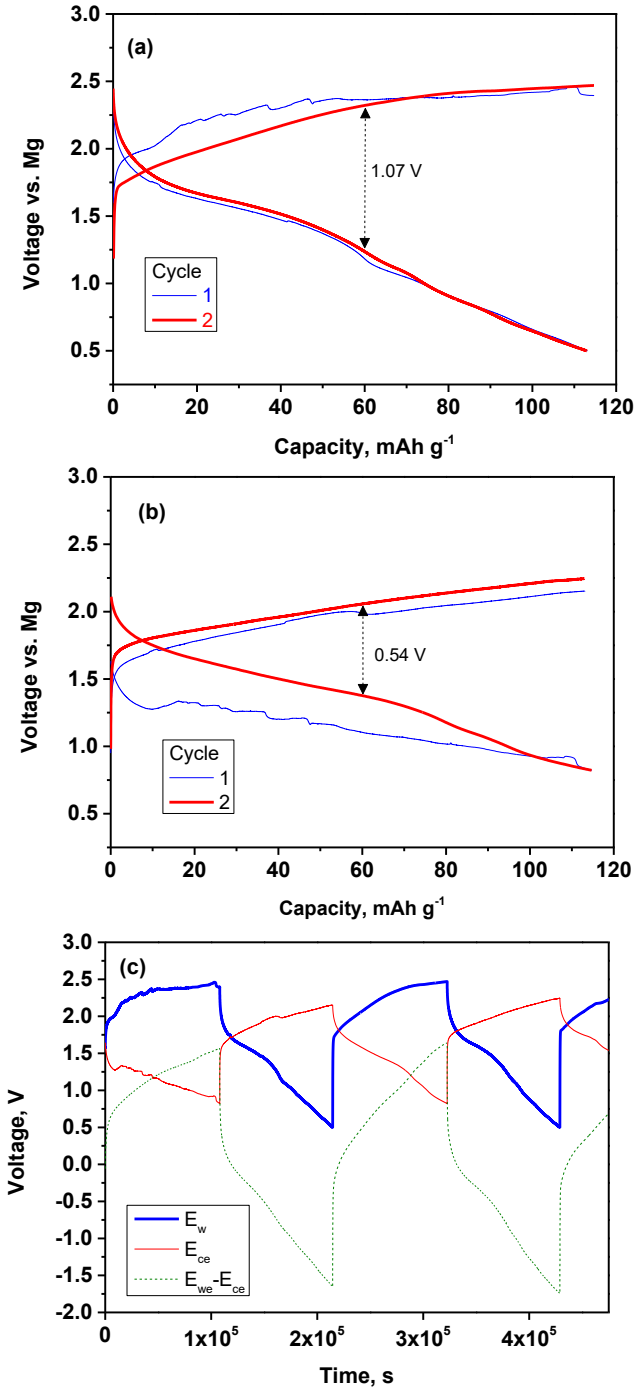

Fig. 5 Voltage curves obtained in galvanostatic experiment in a concentration cell at 4 mA g^{-1} of current intensity. (a) Voltage-capacity for the cathode (initially $MgMn_2O_4$). (b) Voltage-capacity for the anode (initially $Mg_{0.3}Mn_2O_4$). (c) Voltages-time curves. Electrolyte: $Mg(ClO_4)_2$ in ACN. The polarization is marked like the difference between the voltage of the charge and the voltage of the discharge.

The previous demagnesiation by acid-treatment of $MgMn_2O_4$ allows to build an electrochemical device initially using $MgMn_2O_4$ as a positive electrode and $Mg_{0.3}Mn_2O_4$ as a negative electrode, and then working within the more convenient range of composition and within the stability of the electrolyte solution, $MgClO_4$ in ACN. Since both electrode active materials are manganese oxide with different concentrations of magnesium ions, this electrochemical device can be regarded as a concentration cell.

The voltage curves obtained in a concentration cell with magnesium-based electrolyte solution are shown in Fig. 5. The ratio between the masses of the two electrodes is $m_+/m_- = 1.03$. The voltages of both electrodes were monitored against Mg. The electrochemical cycling was initiated with oxidation at the positive electrode ($MgMn_2O_4$) and reduction at the negative electrode ($Mg_{0.3}Mn_2O_4$), and in this way the formation of $Mg_2Mn_2O_4$ and MnO_2 was avoided. The formation of rock-salt structure (Mg_2MnO_4) can be avoided with this cell as it wished, because this phase can inhibit the intercalation of magnesium and would be deleterious for the electrochemical cycling. Thus, the electrochemical cycling should not start by reduction of $MgMn_2O_4$.

The charge of the positive electrode approximately happens from 1.6 to 2.4 V (Fig. 5a), while the discharge is from 2.4 to 0.5 V. The discharge of the negative electrode takes place from 1.6 to 0.8 V (Fig. 5b), and the charge from 0.8 to 2.2 V. Consequently, the charge-discharge of the whole cell is between 1.6 and -1.6 V (Fig. 5c). The voltage polarization deviates the experimental voltage from the theoretically calculated value. Interestingly, the polarization is higher in the voltage curve of the positive electrode (raw spinel) compared to the negative electrode (acid-treated spinel), and this fact is also observed after further electrochemical cycling and with higher current intensity (Fig. 6). The main contribution to the polarization is the oxidation of the cathode, and the reason for that could be the difficult diffusion of magnesium in the Mg-rich $MgMn_2O_4$ spinel due to the lack of vacancies.

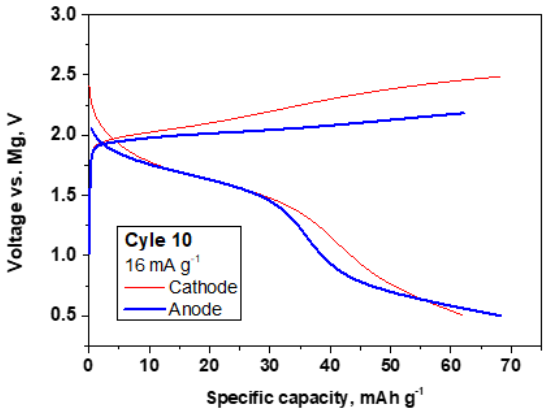

Fig. 6 Voltage-capacity curve after 10 cycles the concentration cell. Lower polarization can be observed for the negative electrode (acid-treated spinel).

The initial reversible capacity referred to the mass of the positive electrode active material is 117 mAh g^{-1} (Fig. 7). This capacity value decreases at higher current intensity. The compositions during the cycling change a maximum of ca. 0.4

Mg per formula unit. In addition, one can observe that certain small fluctuations observed particularly in the voltage curve of the first cycle are due to the reference electrode (Mg), because similar fluctuations are observed simultaneously at both the positive and negative electrode.

The polarization observed in the voltage-capacity curve is lower for the acid-treated spinel, and this result is in good agreement with the presence of cationic vacancies. The relatively rapid voltage decreasing after 35-50 mAh g^{-1} of reduction observed at the two electrodes after several cycles (Fig. 6) could be related with the higher occupancy of Mg sites. The concentration cell can help to minimize the interference in the electrochemistry of effects due to the reference electrode or counter electrode. The reversible charge/discharge process of this concentration cell is a proof of the reversible intercalation of magnesium ion in the framework of the manganese oxide with cubic structure. The results confirm the potential application of the oxy-spinel to perform electrochemical cycling (Fig. 7). The thermodynamic instability of the intermediate compositions $Mg_{1-x}Mn_2O_4$ ($0 < x < 1$) could be the main drawback for their application. We cannot discard the decomposition of ACN molecules on the surface of the manganese oxide particles as it was reported by Kim et al.,[14] and it would contribute to a lower coulombic efficiency and the capacity fading. Through more adequate combination of active materials for the positive and negative electrodes, and further optimization of the electrolyte solution, a veritable magnesium ion battery could be developed. For example, the working voltage of the positive electrode should be higher. An option may be to partially replace manganese by other elements to rise the voltage and stabilizing the intermediate compositions.

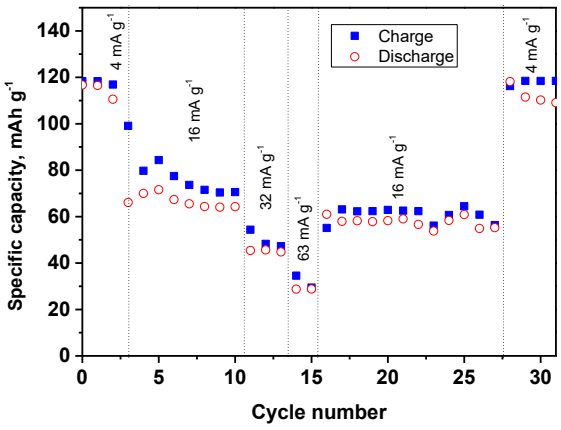

Fig. 7 Capacity as a function of cycle number with variable current intensity.

Percolation and vacancies

To shed light on the effect of the cationic vacancies and the acid-treatment, the percolation energy of Mg^{2+} in the spinel framework has been calculated. First of all, we have analysed the effect of the unit cell parameter in the percolation energy for the acid-treated sample $Mg_{0.3}Mn_2O_4$.(Fig. 8). As expected, if the size of the cell increases, there are more empty space for the cation diffusion, and thus the percolation energy decreases. Secondly, in order to see if the Mg content can affect the percolation energy, we also calculated the percolation energy for $MgMn_2O_4$, $Mg_{0.5}Mn_2O_4$, and Mn_2O_4. Although the volume of the cell progressively decreases from 77.8 to 67.8 $Å^3$ per formula unit, the percolation energy decreases (2.43, 1.34, and 0.80 eV, respectively) as the Mg content decreases, as it allows a better diffusion of the cations.

More interesting is the effect of the possible vacancies created by the acid treatment. The Mn vacancies give rise to an important decrease of the percolation energy (Fig. 8, open circles), while the hypothetical oxygen vacancies result just in the opposite effect (Fig. 8, filled circles). The small content of Mg in the sample $Mg_{0.3}Mn_2O_4$, and the acid treatment causing Mn vacancies, can justify the smaller charge-discharge polarization, as compared with $MgMn_2O_4$. These calculated values of percolation energy can give an idea of the variation of the cation diffusion with the content of Mg and with the manganese vacancies.

We think that the creation of Mn-vacancies could contribute to stabilize the spinel framework and to avoid the collapse of the structure caused by Mg (des)insertion and Jahn-Teller distortion in MnO_6 octahedra. Probably this hypothesis will deserve future studies to be corroborated. It is worth to note here that Sun et al. pointed out that the creation of manganese vacancies is important for the conversion from layered structure to spinel structure.[5] Similarly, Koketsu et al. reported that the introduction of titanium vacancies allows greater capacity for magnesium intercalation in anatase (TiO_2).[27]

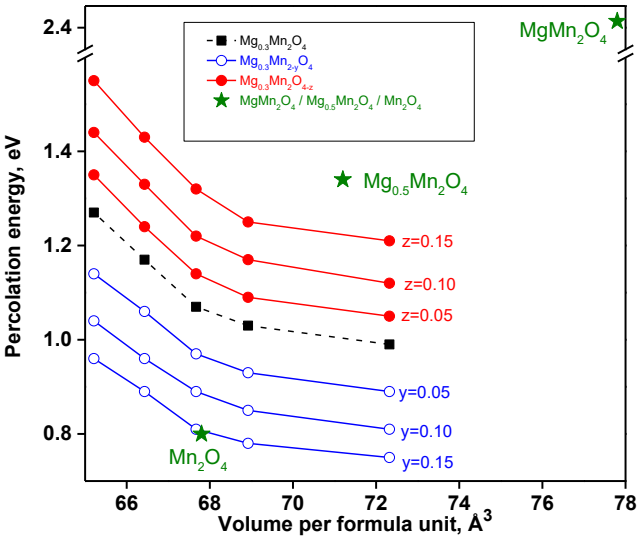

Fig. 8 Calculated percolation energy for several stoichiometries of the cubic oxy-spinel.

Conclusions

The XRD, ESR and XRF results confirm that Mg and Mn ions can be extracted from $MgMn_2O_4$ through disproportionation reaction of Mn(III) in acid solution. After acid treatment of

tetragonal $MgMn_2O_4$, the XRD results show a loss of crystallinity and transformation into cubic phase with lower concentration of Mg. A concentration cell based on two manganese oxide electrodes with different concentration of magnesium ion has been build and tested. The observed charge/discharge process in the concentration cell agrees very well with reversible intercalation of magnesium ion in the spinel-type structure. The creation of cationic vacancies (manganese and magnesium) in the acid-treated spinel decreases the polarization of the voltage curve during the electrochemical charge-discharge. These finds open new possibilities to explore the intercalation of divalent ions in other host materials, and the impact of the creation of cation vacancies, using concentration cells and theoretical calculations.

Author contributions

Alejandro Medina: Investigation. **Ana I. Rodríguez**: Investigation. **Carlos Pérez-Vicente**: Formal analysis, Funding acquisition, Writing-review & editing. **Ricardo Alcántara**: Conceptualization, Methodology, Investigation, Writing – original draft, Writing – review & editing.

Conflicts of interest

There are no conflicts to declare.

Acknowledgements

This work was supported by MINECO (grant number MAT2017–84002-C2–1-R), FEDER funds and Junta de Andalucía (research group FQM288). We also express thanks to the IUNAN for facilitating scientific instruments (XRD and XRF).

Notes and references

1 Y. Liang, H. Dong, D. Aurbach and Y. Yao, *Nat. Energy*, 2020, **5**, 646-656.
2 P. Canepa, G. S. Gautam, D. C. Hannah, R. Malik, M. Liu, K. G. Gallagher, K. A. Persson and G. Ceder, *Chem. Rev.*, 2017, **117**, 4287-4341.
3 M. Liu, Z. Rong, R. Malik, P. Canepa, A. Jain, G. Ceder and K. A. Persson, *Energy Environ. Sci.*, 2015, **8**, 964-974.
4 C. Miralles and R. Gómez, *Electrochem. Commun.*, 2019, **106**, 106512-106516.
5 X. Sun, V. Duffort, B. L. Mehdi, N. D. Browning and L. F. Nazar, *Chem. Mater.*, 2016, **28**, 534-542.
6 M. Cabello, R. Alcántara, F. Nacimiento, G. Ortiz, P. Lavela and J. L. Tirado, *CrystEngComm*, 2015, **17**, 8728-8735.
7 J. C. Knight, S. Therese and A. Manthiram, *ACS Appl. Mater. Interfaces*, 2015, **7**, 22953-22961.
8 S. Okamoto, T. Ichitsubo, T. Kawaguchi, F. Oba, S. Yagi, K. Shimokawa, N. Goto, T. Doi and E. Matsubara, *Adv. Sci.*, 2015, **2**, 1500072-1500081.
9 C. Kim, P. J. Phillips, B. Key, T. Yi, D. Nordlund, Y. S. Yu, R. D. Bayliss, S. H. Han, M. He, Z. Zhang, A. K. Burrell, R. F. Klie and J. Cabana, *Adv. Mater.*, 2015, **27**, 3377-3384.
10 S. Tao, W. Huang, Y. Liu, S. Chen, B. Qian and L. Song, *J. Mater. Chem A*, 2018, **6**, 8210-8214.
11 J. Yin, A. B. Brady, E. S. Takeuchi, A. C. Marschilok and K. J. Takeuchi, *ChemComm*, 2017, **53**, 3665-3668.
12 H. Kobayashi, K. Yamaguchi and I. Honma, RSC Adv., 2019, **9**, 36434-36439.
13 K. Ariyoshi and S. Masuda, *PhysChemChemPhys*, 2020, **22**, 4677-4684.
14 J. S. Kim, W. S. Chang, R. H. Kim, D. Y. Kim, D. W. Han, K. H. Lee, S. S. Lee and S. G. Doo, *J. Power Sources*, 2015, **273**, 210-215.
15 R. Zhang, X. Yu, K. W. Nam, C. Ling, T. S. Arthur, W. Song, A. M. Knapp, S. N. Ehrlich, X. Q. Yang and M. Matsui, *Electrochem. Commun.*, 2012, **23**, 110-113.
16 M. Asif, M. Rashad, Z. Ali, H. Qiu, W. Li, L. Pan and Y. Hou, *Mater. Today*, 2018, **10**, 108-117.
17 K. W. Nam, S. Kim, S. Lee, M. Salama, I. Shterenbeg, Y. Gofer, J. S. Kim, E. Yang, C. S. Park, J. S. Kim, S. S. Lee, W. S. Chang, S. G. Doo, Y. N. Jo, Y. Yung, D. Aurbach and J. W. Choi, *Nano Lett.*, 2015, **15**, 4071-4079.
18 M. Salama, I. Shterenberg, H. Gizbar, N. N. Eliaz, M. Kosa, K. Keinan-Adamsky, M. Afri, L. J. W. Shimon, H. E. Gottlieb, D. T. Major, Y. Gofer and D. Aurbach, *J. Phys. Chem. C*, 2016, **120**, 19586-19594.
19 S. J. Clark, M. D. Segall, C. J. Pickard, P. J. Hasnip, M. J. Probert, K. Refson and M. C. Payne. *Kristallogr.* 2005, **220**, 567-570.
20 G. S. Gautham, P. Canepa, A. Urban, S. H. Bo and G. Ceder. *Chem. Mater.*, 2017, **29**,7918-7930.
21 L. Malavasi, P. Ghigna, G. Chiodelli, G. Maggi and G. Flor, *J. Solid State Chem.*, 2002, **166**, 171-176.
22 C.C. Azzoni, M.C. Mozzati, L. Malavasi, P. Ghigna and G. Flor, *Solid State Commun.*, 2001, **119**, 591-595.
23 X. Lasheras, M. Insauti, J. Martínez de la Fuente, I. Gil de Muro, I. Castellanos-Rubio, L. Marcano, M.L. Fernández-Gubieda, A. Serrano, R. Martín-Rodríguez, E. Garaio, J. A. García and L. Lezama, *Dalton Trans.*, 2019, **48**, 11480-11491.
24 V. Massarotti, D. Capsoni, M. Bini, C. B. Azzoni and A. Paleari, *J. Solid State Chem.*, 1997, **128**, 80-86.
25 R. Sun, P. Jakes, S. Taranenko, H. Kungl and R. A. Eichel, *Solid State Ionics*, 2018, **325**, 201-208.
26 R. Sun, P. Jakes, S. Eurich, D. van Holt, S. Yang, M. Homberger, U. Simon, H. Kungl and R. A. Eichel, *Appl. Magn. Reson.*, 2018, **49**, 415-427.
27 T. Koketsu, J. Ma, B. J. Morgan, M. Body, C. Legein, W. Dachraoui, M. Giannini, A. Demortière, M. Salanne, F. Dardoize, H. Groult, O. J. Borkiewicz, K. W. Chapman, P. Strasser and D. Dambournet, *Nat. Mater.*, 2017, **16**, 1142-1148.